Atmos. Chem. Phys., 11, 3757–3771, 2011
www.atmos-chem-phys.net/11/3757/2011/
doi:10.5194/acp-11-3757-2011

Atmospheric Chemistry and Physics

Dynamical states of low temperature cirrus

D. Barahona[1,*] **and A. Nenes**[1,2]

[1]School of Chemical and Biomolecular Engineering, Georgia Institute of Technology, Atlanta, GA, USA
[2]School of Earth and Atmospheric Sciences, Georgia Institute of Technology, Atlanta, GA, USA
[*]now at: NASA Goddard Space Flight Center, Greenbelt, MD, USA

Received: 28 November 2010 – Published in Atmos. Chem. Phys. Discuss.: 20 December 2010
Revised: 4 April 2011 – Accepted: 4 April 2011 – Published: 26 April 2011

Abstract. Low ice crystal concentration and sustained in-cloud supersaturation, commonly found in cloud observations at low temperature, challenge our understanding of cirrus formation. Heterogeneous freezing from effloresced ammonium sulfate, glassy aerosol, dust and black carbon are proposed to cause these phenomena; this requires low updrafts for cirrus characteristics to agree with observations and is at odds with the gravity wave spectrum in the upper troposphere. Background temperature fluctuations however can establish a "dynamical equilibrium" between ice production and sedimentation loss (as opposed to ice crystal formation during the first stages of cloud evolution and subsequent slow cloud decay) that explains low temperature cirrus properties. This newly-discovered state is favored at low temperatures and does not require heterogeneous nucleation to occur (the presence of ice nuclei can however facilitate its onset). Our understanding of cirrus clouds and their role in anthropogenic climate change is reshaped, as the type of dynamical forcing will set these clouds in one of two "preferred" microphysical regimes with very different susceptibility to aerosol.

1 Introduction

Cirrus clouds are composed of ice crystals that form at high altitudes and temperatures typically below 235 K (Pruppacher and Klett, 1997). They play a key role in climate by modulating the planetary radiative balance (Liou, 1986) and heat transport in the upper troposphere (Ramanathan and Collins, 1991). They strongly impact water vapor transport across the tropopause level (Jensen and Pfister, 2004) and play an important role in lower stratospheric chemistry (Peter, 1997). Cirrus may be affected by aircraft emissions (Seinfeld, 1998) and long range transport of pollutants and play an important (but highly uncertain) role in anthropogenic climate change.

A key microphysical parameter required for understanding the climate impact of cirrus is their concentration of ice crystals, N_c. At temperatures between 200 and 235 K cirrus ice crystals form primarily by homogenous freezing of supercooled deliquesced aerosol (DeMott et al., 2003; Heymsfield and Sabin, 1989), which occurs if the saturation ratio with respect to ice, S, (i.e., the ratio of water vapor partial pressure to its equilibrium value over ice) reaches a characteristic threshold value, S_{hom} (Koop et al., 2000). Heterogeneous freezing of water upon existing aerosol particles (termed "ice nuclei", IN) can also occur (at S lower than S_{hom}) and contribute to ice crystal concentrations (DeMott et al., 2003; Froyd et al., 2009), especially in polluted and dust-rich regions (Barahona et al., 2010a; Haag et al., 2003). The level of water vapor supersaturation (i.e., $S-1$) is the thermodynamic driver for ice formation, and is generated by expansion of air parcels forced by large scale dynamics, gravity waves, and small scale turbulence (Kim et al., 2003).

At temperatures below 200 K (typically near the tropical tropopause layer, TTL) the simple conceptual model for cirrus formation presented above is at odds with observations (Jensen et al., 2010; Krämer et al., 2009; Peter et al., 2006). Temperature fluctuations from mesoscale gravity waves are common at high altitudes and can produce localized vertical motion with updraft velocity as large as $1\,m\,s^{-1}$ (Bacmeister et al., 1999; Herzog and Vial, 2001; Jensen and Pfister, 2004; Sato, 1990). Such motion can increase the rate of expansion cooling at the point of freezing so that a large number of ice crystals is nucleated before the local supersaturation is depleted by ice crystal growth. Homogeneous freezing driven by gravity wave motion would produce high ice crystal number concentration, N_c, between 1 and $10\,cm^{-3}$

Correspondence to: A. Nenes
(athanasios.nenes@gatech.edu)

near the TTL (Barahona et al., 2010a). Such high concentrations however are not observed; N_c remains low, sometimes even lower (0.005–0.2 cm^{-3}) than concentrations observed in weak updraft zones at cold temperatures (Krämer et al., 2009; Lawson et al., 2008). This "low N_c" paradox is accompanied by other phenomena, such as low supersaturation relaxation times (Krämer et al., 2009), which in turn leads to sustained supersaturation levels inside clouds (i.e., "the supersaturation puzzle") (Gao et al., 2004; Krämer et al., 2009; Peter et al., 2006), high clear-sky supersaturation (Jensen et al., 2005), and broad ice crystal size distributions (i.e., large crystal sizes, Jensen et al., 2008). These phenomena occur despite the strong dynamical forcing and the ample amounts of deliquesced aerosol available for homogeneous freezing. Suppressed freezing by organics (Murray, 2008), slow water vapor transfer to the ice phase (Gao et al., 2004; Magee et al., 2006), and freezing to cubic instead of hexagonal ice (Murray et al., 2005), have been proposed to explain these features. These mechanisms are however not capable of explaining the low N_c in low temperature cirrus clouds (Peter et al., 2006). Lacking the predictive understanding of such phenomena hinders the ability of climate models to capture the climate effects of cirrus clouds and their response to anthropogenic perturbations.

Heterogeneous freezing of IN as the main path of cirrus formation has been proposed to explain the features of cirrus clouds at low temperature (Abbatt et al., 2006; Jensen et al., 2010; Murray et al., 2010). Owing to their ability to freeze ice at much lower supersaturation than homogeneous freezing requires, IN can deplete water vapor, reduce supersaturation and inhibit homogeneous freezing; this can drastically reduce the number of ice crystals that forms in the cirrus (Barahona and Nenes, 2009b; DeMott et al., 1994; Kärcher et al., 2006). Much of the anthropogenic impact on cirrus clouds and climate is thought to occur through this IN-N_c feedback mechanism (Lohmann and Feichter, 2005). Dust (Khvorostyanov et al., 2006), effloresced ammonium sulfate (Abbatt et al., 2006; Jensen et al., 2010; Wise et al., 2010), and glassy aerosol (Murray et al., 2010) have been identified as potential heterogeneous IN at the TTL .

The evolution of cirrus clouds at low T has been addressed in several studies. Using a one dimensional (1-D) cloud model, Jensen and Pfister (2004) found that the superposition of temperature fluctuations along Lagrangian trajectories near the TTL resulted in rapid cooling cycles that increased the rate of crystal production by homogeneous nucleation leading to N_c above 1 cm^{-3}. Khvorostyanov et al. (2006) used a 1-D cirrus model to investigate the evolution of a cirrus layer initialized at 200 K and found that regardless of the predominant nucleation mechanism, temperature fluctuations increased the maximum N_c in the cloud (up to 0.6 cm^{-3}). N_c however rapidly decreased after the initial freezing pulse due to the vertical advection of ice crystals precluding new nucleation events and diluting N_c down to about 0.05 cm^{-3}. Gensch et al. (2008) used box model simulations along Lagrangian trajectories to test homogeneous and heterogeneous nucleation scenarios in the formation of cirrus at low T. It was found that only heterogeneous nucleation scenarios (with prescribed IN number concentration around 0.1 cm^{-3}) would result in N_c close to observations. This conclusion was echoed by Froyd et al. (2009) and Jensen et al. (2010) using 1-D models along prescribed T trajectories.

The formation of cirrus clouds however exhibits complex non-linear behavior that may not be captured by box and 1-D models. Ice falling through active freezing zones (typically located at the top of the cirrus layer, Spichtinger and Gierens, 2009b) in clouds consume water vapor and can inhibit homogeneous freezing much like IN do (Kay et al., 2007; Spichtinger and Gierens, 2009b). Their effectiveness depends on their residence time in freezing zones and hence depends on their size. Large ice crystals tend to quickly fall out of freezing zones and have limited effect on new ice formation events; small crystals (typically those with terminal velocity, u_{term}, less or equal to the mean updraft $\overline{u}$ of the cirrus layer) fall slowly and can remain long enough in the upper part of the cloud to affect new freezing events. This suggests that at low temperatures, preexisting (and typically small, Krämer et al., 2009) ice crystals may locally dehydrate the freezing zone sufficiently to inhibit the formation of new ice. The rate of crystal production is not uniform through the freezing zone, as the "local" saturation ratio, S, and updraft velocity, u (defined at the scale of individual cloud "parcels" $\sim 10^0$–10^2 m, Pruppacher and Klett, 1997) may be affected by fluctuations in wind speed and temperature induced by gravity waves (Jensen et al., 2010; Kärcher and Haag, 2004; Kim et al., 2003). These internal S variations are usually neglected in cirrus cloud studies on the basis that the long-term evolution of the cloud is determined by the mean values of S and u.

In this work we analyze the range of conditions for which heterogeneous freezing may explain the features of cirrus clouds at low temperature, and propose an alternative view (based on a statistical description of cirrus formation and evolution) in which the interplay of temperature fluctuations, and ice crystal production and sedimentation leads to previously unidentified natural cirrus states of low ice crystal concentration and sustained high supersaturation.

2 Heterogeneous freezing at low temperature

The impact of IN on N_c depends on their concentration, N_{IN}. If too low ($N_{IN} < 1 \times 10^{-4}$ cm^{-3}), a negligible impact is seen on N_c, as too few (heterogeneously-frozen) ice crystals form to quench supersaturation below the homogeneous/heterogeneous freezing threshold (Barahona and Nenes, 2009b). Low N_c favors large crystal size and therefore heterogeneously frozen ice crystals may sediment out of the cloud layer before significantly modifying S (Spichtinger

and Gierens, 2009a). When N_{IN} approaches a characteristic "limiting" concentration (which depends on updraft velocity, the IN freezing threshold and size), N_{lim}, supersaturation is quenched, homogeneous freezing is suppressed, and N_c decreases steeply (Barahona and Nenes, 2009b). For $N_{IN} \geq N_{lim}$, homogeneous nucleation is inhibited and $N_c = N_{IN}$. Thus, N_{lim} is the minimum N_c that can form in an active nucleation zone in a freshly-formed cirrus cloud (Barahona and Nenes, 2009b) and presents the maximum reduction in N_c possible from IN.

Figure 1 shows N_c accounting for the competition between homogeneous and heterogeneous freezing during cloud formation (Barahona and Nenes, 2009b) (details of the calculation are described Sect. 3.3). As N_c is strongly influenced by the vertical velocity at the point of freezing and much less sensitive to small T variations, the curves in Fig. 1 represent the peak N_c that would be obtained in box models after a single freezing event (Barahona and Nenes, 2008; Hoyle et al., 2005; Kärcher and Lohmann, 2002; Spichtinger and Gierens, 2009a). If N_{IN} is always very close to N_{lim}, competition between homogeneous and heterogeneous freezing could yield N_c close to observations. This requires $N_{IN} \sim 0.1\,cm^{-3}$, which is 20-fold higher than measured dust concentrations ($\sim .005\,cm^{-3}$) at the tropopause level (Froyd et al., 2009). Ammonium sulfate aerosol is present at much higher concentrations than dust, and can serve as IN (Abbatt et al., 2006; Wise et al., 2010) if a fraction of them is effloresced (which is possible, given that it deliquesces at ~90% relative humidity) (Fountoukis and Nenes, 2007; Shilling et al., 2006).

To inhibit homogeneous freezing and reproduce observations of N_c, the concentration of ammonium sulfate IN needs to be within 10% of N_{lim}; if concentrations fall below $0.9N_{lim}$, homogeneous freezing is triggered and predicted N_c is significantly above observations (Fig. 1). If higher concentration than N_{lim} is present, homogeneous freezing is completely suppressed, but too many crystals still form (Barahona and Nenes, 2008). In fact, if all ammonium sulfate is available as IN, N_c from heterogeneous freezing and pure homogeneous freezing are always comparable (Fig. 2), because crystals formed from ammonium sulfate IN are very small (with size close to the dry aerosol; 0.02–0.05 µm, Froyd et al., 2009) and grow too slowly to quench supersaturation before a large fraction of the aerosol freezes heterogeneously. N_c is within observed values only if the average size of crystals at the point of freezing is 2 µm or larger (Fig. 2), which is too large for upper tropospheric aerosol (Froyd et al., 2009). Experimental studies suggest that heterogeneous freezing of ammonium sulfate IN at $T \sim 240$ K can be very selective (about 1 in 10^5 particles nucleate ice, Shilling et al., 2006). If the same selectivity maintains at lower T, too few IN would be available to prevent homogeneous freezing (therefore resulting in high N_c). Higher nucleation selectivity (e.g., about 1 in 10^2 particles actively nucleating ice) would result in complete inhibition of homogeneous freezing and still maintain N_c close to observations (not shown). A pure

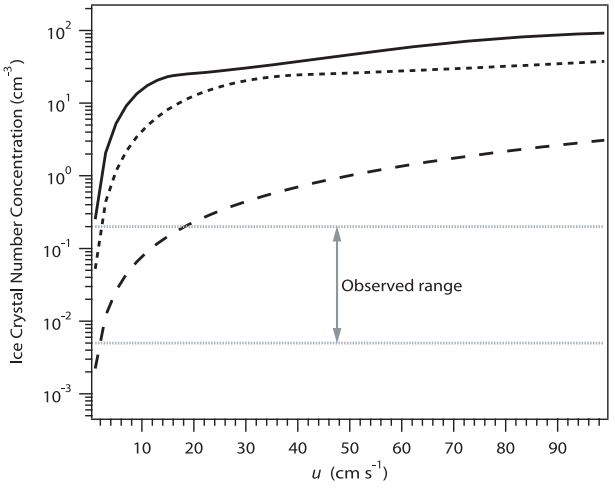

Fig. 1. Ice crystal concentration, N_c, as a function of updraft velocity, u. The cloud was assumed to form at $T = 185$ K and $p = 100$ hPa (details provided in Sect. 3.3.1). Low values of u correspond to cloud formation driven primarily by large scale dynamics, whereas $u > 50\,cm\,s^{-1}$ is characteristic of cirrus developing in the vicinity of convective systems with intense gravity wave breaking (Kim et al., 2003). Solid line indicate N_c calculated for pure homogeneous freezing, dashed line for $N_{IN} = N_{lim}$, and dotted for $N_{IN} = 0.75N_{lim}$. For $N_{IN} = N_{lim}$, N_c lies close to the observed values for $u < 50\,cm\,s^{-1}$ (Krämer et al., 2009) but is very sensitive to small fluctuations in N_{IN}.

heterogeneous scenario of ice nucleation on ammonium sulfate however implies a maximum supersaturation below 20% (Fig. 3b), i.e., S greater than 1.2 would be rarely observed as newly formed crystals would rapidly remove supersaturation. This is at odds with observations of relative humidity that suggest that clear-sky supersaturation in the vicinity of cirrus up to 70% (and occasionally above) is very common at low temperature (Krämer et al., 2009). Hence the low N_c and high S observed at high-level cirrus can be reconciled with box-model results only if the concentration of ammonium sulfate IN is remarkable constant ($0.1 \pm 0.01\,cm^{-3}$), the concentration of dust is exceptionally large, or, the fluctuations in vertical velocity from gravity wave motion are neglected.

The freezing fraction of organic glassy aerosol can be much lower than that of ammonium sulfate and maintain N_{IN} close to N_{lim} (hence yield low N_c, Fig. 3a) if the vertical velocity is below $15\,cm\,s^{-1}$ (Murray et al., 2010). At larger updrafts however, homogeneous nucleation is triggered, producing high N_c (Fig. 3a). When integrated over a normal distribution of updrafts with standard deviation σ_u (Fig. 3c), N_c remains within observed values for σ_u up to $40\,cm\,s^{-1}$ at $T = 195$ K. The onset of homogeneous nucleation occurs at even lower u for colder temperatures and N_c deviates from observations for σ_u as low as $10\,cm\,s^{-1}$ at $T = 185$ K. Predominance of heterogeneous nucleation from glassy IN would also imply maximum supersaturation around 30% if the new formed ice crystals efficiently remove

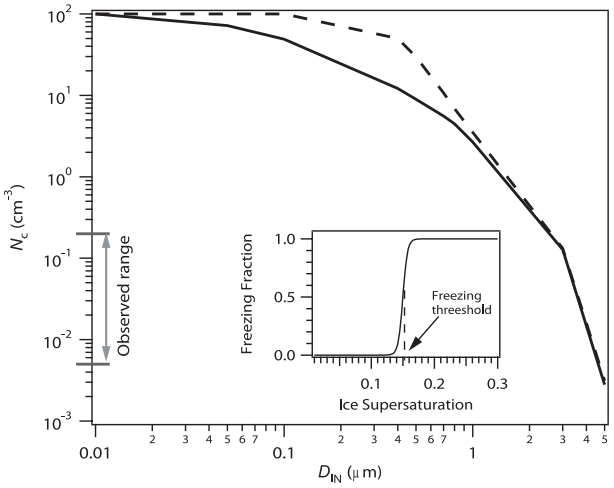

Fig. 2. Simulations of ice crystal concentration by pure heterogeneous freezing. N_c is presented as a function of the initial size of the ice nuclei. Conditions (Lawson et al., 2008) used were $T = 185$ K, $p = 100$ hPa, and vapor-to-ice deposition coefficient, α_d, of 0.07 (dashed line), and 1.0 (solid line). The IN population was assumed to be monodisperse with total number concentration of 100 cm^{-3} (Lawson et al., 2008). Freezing of solid ammonium sulfate was assumed to occur in a "burst" around the heterogeneous freezing threshold described by sigmoidal freezing spectrum with inflection point $S_{het} = 15\%$ (Abbatt et al., 2006), where 99% of the aerosol freeze within a 2% supersaturation interval about S_{het} (inset plot).

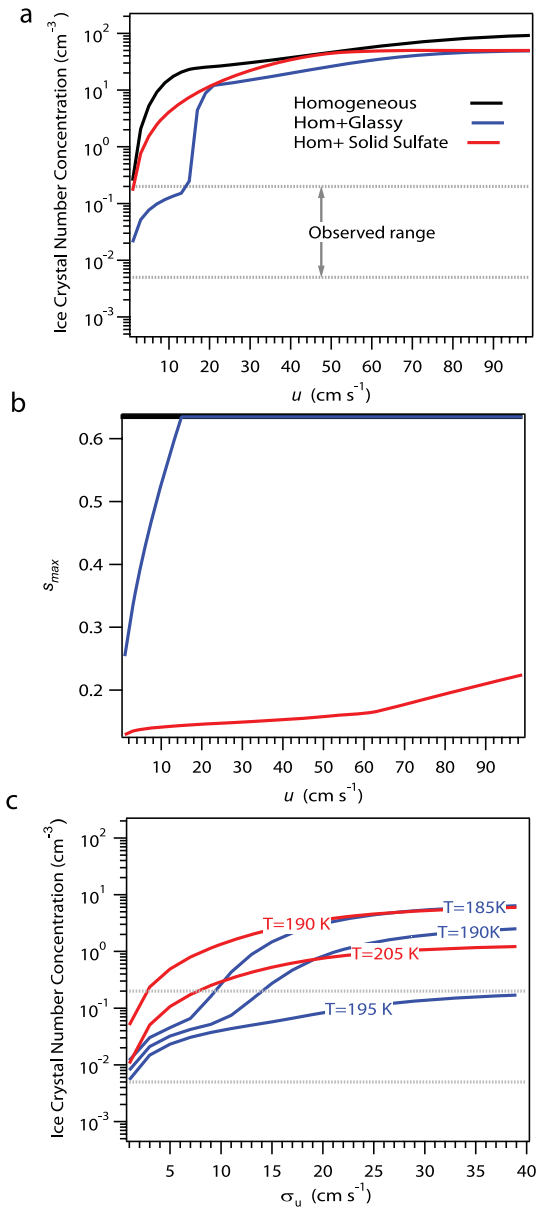

Fig. 3. Comparison between heterogeneous effects from solid ammonium sulfate (Abbatt et al., 2006) and glassy citric acid aerosol (Murray et al., 2010), using the analytical model of Barahona and Nenes (2009a) for homogeneous and heterogeneous freezing. **(a)** Maximum ice crystal concentration as a function of updraft velocity for a single freezing event. **(b)** Maximum supersaturation achieved for a single freezing event. **(c)** Ice crystal concentration averaged over a normal distribution of updraft velocities with zero mean and standard deviation σ_u. The gray lines represent the range of N_c typically observed (Krämer et al., 2009).

supersaturation (Barahona et al., 2010a; Murray et al., 2010). However as the freezing fraction of glassy IN is small, S can increase even after heterogeneous nucleation has occurred. Still, S would have to remain below S_{hom} for N_c to remain low unless homogeneous freezing is suppressed. The later scenario is however not supported by observations. Both, in-cloud and clear-sky RH are generally limited by the homogeneous freezing threshold indicating efficient supersaturation removal by homogeneously-frozen ice crystals (Krämer et al., 2009; Selkirk et al., 2010). Although uncertainty in RH can be typically up to 20% (Krämer et al., 2009), it is still smaller than the difference between the homogeneous and heterogeneous freezing thresholds, typically between 30% and 40%, giving this support to the idea that homogeneous freezing occurs at low temperatures. All together, this implies that in the presence of (ubiquitous) T fluctuations, the presence of glassy IN may contribute, but not fully account for the observed characteristics of low T cirrus.

3 Parcel statistical ensemble model

The main processes affecting the evolution of N_c and mean saturation ratio, S_o, within a cirrus layer are the freezing of new ice, the sedimentation of existing ice crystals, the lifting of air masses (which generates supersaturation), and the relaxation (i.e., mass transfer) of water vapor to/from the ice phase. The magnitude of each process can be expressed in terms of a characteristic timescale, i.e., τ_{fr}, τ_{sed}, τ_{lift}, and τ_{rel} for freezing, sedimentation, lifting, and relaxation, respectively. Fluctuations in S and u can have a strong impact on all cloud processes; we therefore represent them in terms of a

probability distribution centered about the cirrus-average saturation ratio, S_o, and vertical velocity, $\overline{u}$. The width of these probability distributions is largely determined by the mean amplitude of temperature fluctuations, δT (Bacmeister et al., 1999; Hoyle et al., 2005; Kärcher and Burkhardt, 2008). The rate of ice production is given by the frequency with which S exceeds the homogeneous freezing threshold (Kärcher and Burkhardt, 2008) times the length and intensity of each freezing event (hence τ_{fr}) (Barahona and Nenes, 2008; Pruppacher and Klett, 1997). The same fluctuations also affect the local mass transfer rate between the ice and vapor phases, so that when averaged over the cloud, water deposition/sublimation occurs at an "effective" saturation ratio, S_{eff}, that may differ from S_o.

Supersaturation and crystal number in the cirrus cloud are determined using a "Lagrangian statistical ensemble" approach. This involves determining the time-dependant state of i homogeneous Lagrangian "parcels" that move with a (time-dependant) vertical velocity, u_i; ensemble averaging of the parcel solutions (outlined below) weighted by the appropriate probability distribution give approximate equations that describe the time-dependant properties for the whole cirrus. From these considerations, simple equations can be derived that represent the evolution of N_c and S_o in the cirrus (Sects. 3.1, 3.2).

3.1 Evolution of saturation ratio

In the absence of ice nucleation, the rate of change of saturation ratio, S, within the i^{th} Lagrangian parcel is given by (Barahona and Nenes, 2009a; Seinfeld and Pandis, 1998)

$$\frac{dS_i}{dt} = \alpha u_i S_i - \gamma \int_{D_{min}}^{\infty} D_{c,i}^2 \frac{dD_{c,i}}{dt} n_{c,i}(D_c) dD_c \quad (1)$$

where $\alpha = \frac{g\Delta H_s M_w}{c_p R T^2} - \frac{g M_a}{RT}$ and $\gamma = \frac{\rho_i}{\rho_a}\frac{\pi}{2}\frac{M_a p}{M_w p_i^o}$, ΔH_s is the latent heat of sublimation of water, g is the acceleration of gravity, c_p is the heat capacity of air, p_i^o is the ice saturation vapor pressure at T (Murphy and Koop, 2005), p is the ambient pressure, M_w and M_a are the molar masses of water and air, respectively, R is the universal gas constant, ρ_i and ρ_a are the ice and air densities, respectively, and D_c is the volume-equivalent diameter of an ice particle (assuming spherical shape). $n_{c,i}(D_c)$ is the ice crystal size distribution in the i^{th} parcel, and

$$\frac{dD_{c,i}}{dt} = \frac{G(S_i - 1)}{D_{c,i}} \quad (2)$$

where $G \approx \left[\frac{\rho_i RT}{4 p_i^o D_v' M_w} + \frac{\Delta H_s \rho_i}{4 k_a T}\left(\frac{\Delta H_s M_w}{RT} - 1\right)\right]^{-1}$, k_a is the thermal conductivity of air, $D_v' = D_v'(T, p, \alpha_d)$ is the water vapor diffusion coefficient from the gas to ice phase corrected for non-continuum effects, and α_d is the water vapor deposition coefficient. Substituting Eq. (2) into Eq. (1) provides after evaluation of the integral,

$$\frac{dS_i}{dt} = \alpha u_i S_i - \frac{(S_i - 1)}{\tau_{rel,i}} \quad (3)$$

where $\tau_{rel,i} = \left(\beta N_{c,i} \bar{D}_{c,i}\right)^{-1}$ is the relaxation time scale in the i^{th} parcel, $\beta = \gamma G$, and, $N_{c,i}$, $\bar{D}_{c,i}$ are the concentration and mean size of ice crystals in the i^{th} parcel, respectively.

Equation (3) provides the supersaturation "state" for every Lagrangian parcel considered in the ensemble. Knowledge of the distribution of u_i (from the spectrum of gravity waves in the cirrus) can then be used to "drive" the parcels in the ensemble to find the resulting distribution of S_i. Averaging is carried out first over all parcels reaching a given cloud level with vertical velocity u_j (referred to as the "j^{th} cloud velocity state"), and then averaging over all cloud states. Based on this, the average saturation ratio, S_o, of the cloud over a time interval Δt is

$$S_o(t) = \int_{-\infty}^{+\infty} \int_{X(t)} \int_{0}^{1} S_i(\mu, \tilde{x}, \tau) P(\mu, \tilde{x}, \tau) d\tau d\tilde{x} d\mu \quad (4)$$

where $\mu = \frac{u}{\bar{u}}$, u and $\bar{u}$ are the instantaneous and average vertical velocity, respectively, $\tilde{x}$ denotes the position in the cloud, $\tau = \frac{t'}{\Delta t}$, where t' is the averaging time, and $X(t)$ is the domain of $\tilde{x}$. $P(\mu, \tilde{x}, \tau)$ is the normalized probability at time t' of finding a parcel between position $\tilde{x}$ and $\tilde{x} + d\tilde{x}$ (where $d\tilde{x} = \frac{dxdydz}{V_{cloud}}$), with vertical velocity within u and $u + du$.

Equation (1) can be simplified, by considering that fluctuations generated by gravity waves are random in nature (i.e., follow a Gaussian distribution, Fig. 4d). Thus, under the assumption that $P(\mu, \tilde{x}, \tau)$ does not vary with space and time over Δt, $P(\mu, \tilde{x}, \tau) \simeq P(\mu)$ and Eq. (4) simplifies to

$$S_o(t) = \int_{-\infty}^{+\infty} \int_{X(t)} \int_{0}^{1} S_i(\mu, \tilde{x}, \tau) P(\mu) d\tau d\tilde{x} d\mu \quad (5)$$

Equation (5) assumes that S_o is affected by processes that act throughout the volume of the cirrus cloud. Other processes, like entrainment and radiative cooling, are neglected. Although this will not affect the conclusions of our study, they could be included in future studies e.g. indirectly through appropriate modification of the vertical velocity distribution (Barahona and Nenes, 2007).

Defining $\bar{S}_j = \int_{X(t)} \int_{0}^{1} S_i(\mu, \tilde{x}, \tau) d\tau d\tilde{x}$ as the average supersaturation of parcels in the "j" velocity state over the time interval Δt, Eq. (5) can be rewritten as

$$S_o(t) = \int_{-\infty}^{+\infty} \bar{S}_j(\mu_j) P(\mu_j) d\mu_j \quad (6)$$

the time derivative of which gives,

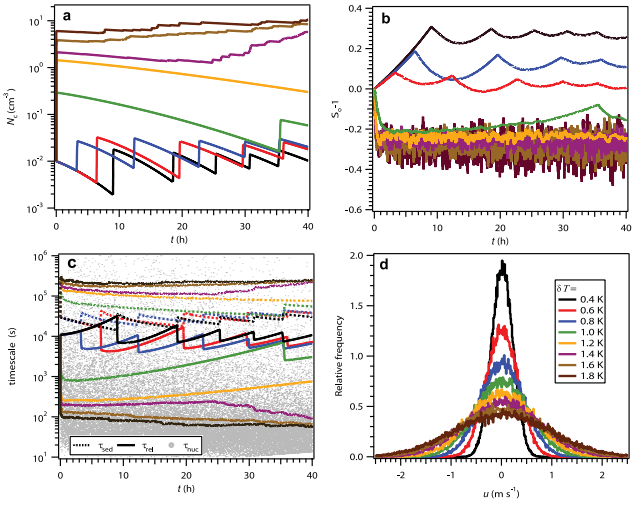

Fig. 4. Evolution of a cirrus cloud under pure homogeneous freezing, lifting at 1 cm s^{-1} with initial $T = 195$ K and cloud thickness, $H = 500$ m, and $\alpha_d = 1$. Shown are **(a)** the ice crystal number concentration, **(b)** mean supersaturation, **(c)** characteristic timescales of freezing (gray dots), relaxation (solid lines), and sedimentation (dotted lines), and, **(d)** frequency distribution of vertical velocity, for different values of the mean amplitude temperature fluctuations, δT.

$$\frac{dS_o}{dt} = \int_{-\infty}^{+\infty} \frac{d\bar{S}_j(\mu_j)}{dt} P(\mu_j) d\mu_j + \int_{-\infty}^{+\infty} \bar{S}_j(\mu_j) \frac{dP(\mu_j)}{dt} d\mu_j \quad (7)$$

the second integral on the right hand side of Eq. (7) depends on the source of vertical velocity fluctuations. Distant sources of gravity waves result in stationary $P(\mu_j)$, hence $\frac{dP(\mu_j)}{dt} \to 0$. However $P(\mu_j)$ can be perturbed by near convective and orographic sources; in such cases $P(\mu_j)$ is not completely Gaussian and exhibits a tail towards high velocities (Bacmeister et al., 1999). For the purpose of this study it is assumed that $\frac{dP(\mu_j)}{dt} = 0$, which implies that the characteristic amplitude of temperature fluctuations, δT, remains constant during the entire period of simulation. Equation (7) then becomes

$$\frac{dS_o}{dt} \approx \int_{-\infty}^{+\infty} \frac{d\bar{S}_j(\mu_j)}{dt} P(\mu_j) d\mu_j \quad (8)$$

Using the definition of $\bar{S}_j$,

$$\frac{d\bar{S}_j}{dt} = \int_{X(t)} \int_0^1 \frac{dS_i(\mu, \tilde{x}, \tau)}{dt} d\tau d\tilde{x} \quad (9)$$

Substitution of Eq. (3) into above provides

$$\frac{d\bar{S}_j}{dt} = \int_{X(t)} \int_0^1 \left\{ \alpha u_j S_i - \frac{(S_i - 1)}{\tau_{\mathrm{rel},i}} \right\} d\tau d\tilde{x} = \alpha u_j \int_{X(t)} \int_0^1 S_i d\tau d\tilde{x} - \int_{X(t)} \int_0^1 \left(\frac{S_i - 1}{\tau_{\mathrm{rel},i}} \right) d\tau d\tilde{x} \quad (10)$$

which can be rewritten as,

$$\frac{d\bar{S}_j}{dt} = \alpha u_j \bar{S}_j - \int_{X(t)} \int_0^1 \left(\frac{S_i - 1}{\tau_{\mathrm{rel},i}} \right) d\tau d\tilde{x} \quad (11)$$

Introducing $\bar{S}_{\mathrm{eff},j}$ so that,

$$\int_{X(t)} \int_0^1 \left(\frac{S_i - 1}{\tau_{\mathrm{rel},i}} \right) d\tau d\tilde{x} = \left(\bar{S}_{\mathrm{eff},j} - 1 \right) \int_{X(t)} \int_0^1 \frac{1}{\tau_{\mathrm{rel},i}} d\tau d\tilde{x} \quad (12)$$

From Eq. (3),

$$\frac{1}{\tau_{\mathrm{rel},j}} = \int_{X(t)} \int_0^1 \frac{1}{\tau_{\mathrm{rel},i}} d\tau d\tilde{x} = \left[\beta N_c \bar{D}_c \right]_{\mu = \mu_j} \quad (13)$$

Combining Eqs. (12) and (13), Eq. (11) can be written as

$$\frac{d\bar{S}_j}{dt} = \alpha u_j \bar{S}_j - \frac{\bar{S}_{\mathrm{eff},j} - 1}{\tau_{\mathrm{rel},j}} \quad (14)$$

where $\tau_{\mathrm{rel},j}$ is the relaxation time scale associated with the j^{th} state. $\bar{S}_{\mathrm{eff},j}$ is an "effective" saturation ratio for deposition/sublimation processes, defined below. Introducing Eq. (14) into Eq. (8),

$$\frac{dS_o}{dt} = \int_{-\infty}^{+\infty} \left(\alpha u_j \bar{S}_j - \frac{\bar{S}_{\mathrm{eff},j} - 1}{\tau_{\mathrm{rel},j}} \right) P(\mu_j) d\mu_j \quad (15)$$

or,

$$\frac{dS_o}{dt} = \int_{-\infty}^{+\infty} \alpha u_j \bar{S}_j P(\mu_j) d\mu_j - \int_{-\infty}^{+\infty} \left(\frac{\bar{S}_{\mathrm{eff},j} - 1}{\tau_{\mathrm{rel},j}} \right) P(\mu_j) d\mu_j \quad (16)$$

The first term in the right hand side of Eq. (16) must be equal to $\bar{u} S_o$, as in the absence of deposition/sublimation, S_o in the layer increases exponentially with time (Pruppacher and Klett, 1997). With this, Eq. (16) becomes,

$$\frac{dS_o}{dt} = \frac{S_o}{\tau_{\mathrm{lift}}} - \int_{-\infty}^{+\infty} \left(\frac{\bar{S}_{\mathrm{eff},j} - 1}{\tau_{\mathrm{rel},j}} \right) P(\mu_j) d\mu_j \quad (17)$$

where $\tau_{\mathrm{lift}} = (\alpha \bar{u})^{-1}$. Equation (17) must be solved for each time step specifying $P(\mu_j)$ and then evaluating $\bar{S}_{\mathrm{eff},j}$ and the integral on the right hand side. Since $P(\mu_j)$ is determined

by the random overlapping of gravity waves of different frequency and amplitude (e.g., u_j is given by a Fourier series in time, Sect. 3.3), then for a time step of integration much smaller than $\tau_{\rm lift}$ ($\sim 10^2$ s) Eq. (17) can be approximated by

$$\frac{dS_{\rm o}}{dt} = \alpha \bar{u} S_{\rm o} - \left. \frac{\bar{S}_{{\rm eff},j} - 1}{\tau_{{\rm rel},j}} \right|_{\mu=\mu_j} \tag{18}$$

where $\bar{S}_{{\rm eff},j}$ and $\tau_{{\rm rel},j}$ are calculated at the instantaneous vertical velocity.

Equation (18) gives the evolution of the $S_{\rm o}$ in the cirrus cloud; its solution however requires the knowledge of $\bar{S}_{{\rm eff},j}$. This is accomplished by considering the properties of the different parcels reaching the cloud layer at t. For example, if S_i in the $i^{\rm th}$ parcel is a pseudo-steady state, $\frac{dS_i}{dt} \sim 0$ (Korolev and Mazin, 2003) and from Eq. (3),

$$S_{i,{\rm ss}} = \frac{\tau_{{\rm lift},i}}{\tau_{{\rm lift},i} - \tau_{{\rm rel},i}} \tag{19}$$

where $\tau_{{\rm lift},i} = (\alpha u_i)^{-1}$ and $S_{i,{\rm ss}}$ is the steady state saturation ratio in the $i^{\rm th}$ parcel. If $\tau_{{\rm lift},i} < 0$ then $S_{i,{\rm ss}} < 1$, and vice-versa. Thus, if $u_j < 0$, the layer would likely be subsaturated over Δt (e.g., Eq. 6), and vice-versa when $u_j > 0$. Thus, depending on the sign of u_j there is net deposition/sublimation of water vapor in the cloud layer. Not all parcels however reach steady state; therefore the degree of saturation/subsaturation associated with the $j^{\rm th}$ state depends on the probability distribution of saturation within the cloudy layer, $P_{\rm s}(S, S_{\rm o}, \delta T)$, which is a function of $S_{\rm o}$ and the average amplitude of temperature fluctuations, δT. Thus, $S_{\rm eff}$ for $u_j < 0$ is found by averaging over all states that would lead to subsaturation, i.e., $P_{\rm s}(S, \delta T, S_{\rm o})$ for which $S < 1$. Similarly, when $u_j > 0$, the supersaturated ($S > 1$) region of $P_{\rm s}(S, \delta T, S_{\rm o})$ is used,

$$\bar{S}_{{\rm eff},j} = \frac{\int_{\rm a}^{\rm b} S \frac{dP_{\rm s}(S,\delta T,S_{\rm o})}{dS} dS}{\int_{\rm a}^{\rm b} \frac{dP_{\rm s}(S,\delta T,S_{\rm o})}{dS} dS} \tag{20}$$

$$\text{where} \quad a = \begin{cases} 1 & u_j > 0 \\ 0 & u_j \le 0 \end{cases} \text{ and } b = \begin{cases} S_{\rm hom} & u_j > 0 \\ 1 & u_j \le 0 \end{cases}$$

The homogeneous freezing threshold, $S_{\rm hom}$, is set as the upper limit of $P_{\rm s}(\delta T, S_{\rm o})$ as ice crystal production quickly removes supersaturation above $S_{\rm hom}$ (Kärcher and Burkhardt, 2008; Kärcher and Haag, 2004).

3.2 Evolution of ice crystal number concentration

The evolution of the number concentration within a cloudy layer is given by

$$\frac{dN_{\rm c}}{dt} = \left.\frac{dN_{\rm c}}{dt}\right|_{\rm fr} + \left.\frac{dN_{\rm c}}{dt}\right|_{\rm sed} \tag{21}$$

where $\left.\frac{dN_{\rm c}}{dt}\right|_{\rm fr}$ is the rate production of ice crystals within the layer, and $\left.\frac{dN_{\rm c}}{dt}\right|_{sed}$ is their sedimentation rate. If homogeneous and heterogeneous nucleation are active, $\left.\frac{dN_{\rm c}}{dt}\right|_{\rm fr}$ is given by,

$$\left.\frac{dN_{\rm c}}{dt}\right|_{\rm fr} = \left.\frac{dN_{\rm c}}{dt}\right|_{\rm fr,hom} + \left.\frac{dN_{\rm c}}{dt}\right|_{\rm fr,het}$$

where $\left.\frac{dN_{\rm c}}{dt}\right|_{\rm fr,hom}$ and $\left.\frac{dN_{\rm c}}{dt}\right|_{\rm fr,het}$ are the ice crystal production rates from homogeneous and heterogeneous nucleation, respectively.

3.2.1 Homogeneous nucleation

Ice crystal production by homogeneous nucleation is driven by local motions and occurs within single parcels when $S_i > S_{\rm hom}$. The maximum ice crystal concentration produced by homogeneous freezing within the $i^{\rm th}$ parcel is given by (Barahona and Nenes, 2008; Pruppacher and Klett, 1997)

$$N_{{\rm c},i} = N_{\rm o} \left\{ 1 - \exp\left(- \int_0^{t_{{\rm max},i}} \bar{v}_{\rm o} J(S_i) dt \right) \right\} \tag{22}$$

where $t_{{\rm max},i}$ is the time at which ice crystal nucleation stops, J is the homogeneous nucleation rate coefficient and $N_{\rm o}$, $\bar{v}_{\rm o}$ are the deliquesced aerosol number concentration and average volume, respectively. Taking the time derivative of Eq. (22) gives,

$$\left.\frac{dN_{{\rm c},i}}{dt}\right|_{\rm fr,hom} = N_{\rm o} \bar{v}_{\rm o} J(S_i) \exp\left(- \int_0^{t_{{\rm max},i}} \bar{v}_{\rm o} J(S_i) dt \right) \tag{23}$$

which can be approximated by (Barahona and Nenes 2008)

$$\left.\frac{dN_{{\rm c},i}}{dt}\right|_{\rm fr,hom} \approx N_{\rm o} \bar{v}_{\rm o} J_{{\rm max},i} \exp\left(- \frac{\bar{v}_{\rm o}}{\alpha u_i} \int_0^{S{\rm max}} J(S_i) dS_i \right) \tag{24}$$

where $J_{{\rm max},i} = J(S_{{\rm max},i})$. $S_{{\rm max},i}$ is the maximum saturation ratio reached in the $i^{\rm th}$ parcel, calculated by setting $\frac{dS_i}{dt} = 0$ in Eq. (1),

$$S_{{\rm max},i} = \frac{\gamma}{\alpha u_i} \int_{\bar{D}_{\rm o}}^{\infty} D_{{\rm c},i}^2 \frac{dD_{{\rm c},i}}{dt} n_{i,{\rm nuc}}(D_{\rm c}) dD_{\rm c} \tag{25}$$

where $n_{i,{\rm nuc}}(D_{\rm c})$ is the size distribution of the recently nucleated ice crystals, and $\bar{D}_{\rm o}$ is the mean size of the deliquesced aerosol. Equation (25) assumes that only recently nucleated ice crystals are contained within the parcel. In reality, a fraction of preexisting crystals remain in nucleation zones (typically located near the cloud top, Spichtinger and Gierens, 2009b) inhibiting the homogeneous freezing of ice. Ice crystals experience gravitational settling, hence only those crystals with terminal velocity, $u_{\rm term}$, below $\bar{u}$ would be found at

the cloud top. Adding the consumption of water vapor from preexisting crystals to the right hand side of Eq. (25) gives

$$S_{\max,i} = \frac{\gamma}{\alpha u_i}\left[\int_{\bar{D}_o}^{\infty} D_{c,i}^2 \frac{dD_{c,i}}{dt} n_{i,\mathrm{nuc}}(D_c) dD_c + \int_{D_{\min}}^{D_{\mathrm{term}}} D_c^2 \frac{dD_c}{dt} n_c(D_c) dD_c\right] \quad (26)$$

where $n_c(D_c)$ is the cloud ice crystal size distribution, D_{term} is the size of the crystal for which $u_{\mathrm{term}} = \bar{u}$, and $D_{\min}$ is the minimum size of the preexisting crystals in the cloud. Equation (26) can be combined with Eq. (2) to obtain

$$S_{\max,i} = \frac{\gamma}{\alpha u_i}\left[\int_{\bar{D}_o}^{\infty} D_{c,i}^2 \frac{dD_{c,i}}{dt} n_{i,\mathrm{nuc}}(D_c, S_{\max,i}) dD_c + G N_c \bar{D}_c f_{ps}(S_{\max,i} - 1)\right] \quad (27)$$

where, $f_{ps} = \frac{1}{N_c \bar{D}_c} \int_{D_{\min}}^{D_{\mathrm{term}}} D_c n_c(D_c) dD_c$, is the fraction of preexisting ice crystals remaining in nucleation zones. As ice crystals remaining in the cloud layer were produced by preexisting freezing events, Eq. (27) provides a link between the history of different parcels and the nucleation of new crystals. The analytical solution of Eq. (27) is presented elsewhere (Barahona and Nenes, 2009b; Barahona et al., 2010b).

The rate of ice crystal production by homogeneous nucleation in the j^{th} cloud velocity state is given by the concentration of nucleated crystals over the freezing timescale,

$$\left.\frac{dN_{c,j}}{dt}\right|_{\mathrm{fr,hom}} = \frac{P_s(S > S_{\mathrm{hom}}) N_o}{\tau_{\mathrm{hom},j}} H_v(u_j) \quad (28)$$

where $\tau_{\mathrm{hom},j}^{-1} = \bar{v}_o J_{\max,j} \exp\left(-\frac{\bar{v}_o}{\alpha u_j} \int_0^{S\max} J(S_j) dS_j\right)$. $H_v(u_j)$ is the Heaviside function and is introduced because homogeneous nucleation is very unlikely in parcels with negative vertical velocity (i.e., updraft must be maintained for some time before S_{hom} is reached after which it is quickly depleted by crystal nucleation and growth, Barahona and Nenes, 2008; Kärcher and Lohmann, 2002) . $P_s(S > S_{\mathrm{hom}})$ represents the fraction of parcels for which $S > S_{\mathrm{hom}}$. Using the same averaging procedure as for the supersaturation equation, we obtain

$$\left.\frac{dN_c}{dt}\right|_{\mathrm{fr,hom}} = N_o\, P_s(S > S_{\mathrm{hom}}) \left.\frac{H_v(\mu_j)}{\tau_{\mathrm{hom},j}}\right|_{\mu=\mu_j} \quad (29)$$

3.2.2 Heterogeneous nucleation

The formulation of the ice crystal production rate by heterogeneous freezing is simplified by using the ice nucleation spectrum, $N_{\mathrm{IN}}(S,T)$ (Barahona and Nenes, 2009a) . Assuming that $N_{\mathrm{IN}}(S,T)$ is weakly dependent on T and $N_{\mathrm{IN}}(S,T) = N_{o,\mathrm{het}} f_{\mathrm{het}}(S)$, then following Eq. (29) we write,

$$\left.\frac{dN_c}{dt}\right|_{\mathrm{fr,het}} = N_{o,\mathrm{het}} \frac{df_{\mathrm{het}}}{dS}\frac{dS}{dt}\, P_s(S > S_{\mathrm{het}}) H_v(\mu_j)\big|_{\mu=\mu_j} \quad (30)$$

where, $N_{o,\mathrm{het}}$ is the total number concentration of IN species, and f_{het}, S_{het} its freezing fraction and heterogeneous nucleation threshold, respectively. As N_{IN} is usually small, S is not immediately depleted by ice crystal growth and $\frac{dS}{dt}$ can be approximated by the instantaneous rate of increase of supersaturation (this is further justified in the case of glassy IN as $\frac{df_{\mathrm{het}}(S)}{dS}$ is constant , Murray et al., 2010). Therefore,

$$\left.\frac{dN_c}{dt}\right|_{\mathrm{fr,het}} = N_{o,\mathrm{het}} \frac{df_{\mathrm{het}}}{dS} \alpha u_j S\, P_s(S > S_{\mathrm{het}}) H_v(\mu_j)\big|_{\mu=\mu_j} \quad (31)$$

which can be written as

$$\left.\frac{dN_c}{dt}\right|_{\mathrm{fr,het}} = N_{o,\mathrm{het}} P_s(S > S_{\mathrm{het}}) \left.\frac{H_v(\mu_j)}{\tau_{\mathrm{het},j}}\right|_{\mu=\mu_j} \quad (32)$$

where $\tau_{\mathrm{het},j} = \left(\frac{df_{\mathrm{het}}}{dS} \alpha u_j S\right)^{-1}$.

3.2.3 Sedimentation of ice crystals

Sedimentation processes out of the cloud layer depend primarily on the bulk properties of the cloud, i.e., the mean ice crystal size distribution and number concentration (interaction of individual parcels with falling crystals within the layer is accounted for in Eq. 27). The ice crystal loss rate by sedimentation is then given by,

$$\left.\frac{dN_c}{dt}\right|_{\mathrm{sed}} = \frac{1}{H}\int_{D_{\min}}^{\infty} u_{\mathrm{term}}(D_c) n(D_c) dD_c \quad (33)$$

where H is the cloud layer thickness. As $u_{\mathrm{term}} \sim D_c$ (Heymsfield and Iaquinta, 2000), Eq. (33) can be further simplified to

$$\left.\frac{dN_c}{dt}\right|_{\mathrm{sed}} = \frac{N_c \bar{u}_{\mathrm{term}}}{H} = \frac{N_c}{\tau_{\mathrm{sed}}} \quad (34)$$

where $\bar{u}_{\mathrm{term}} = u_{\mathrm{term}}(\bar{D}_c)$.

3.3 Numerical solution

3.3.1 Competition between homogeneous and heterogeneous freezing

Calculation of ice crystal number concentration, N_c in in-situ cirrus from combined homogeneous and heterogeneous nucleation in Figs. 1 and 3 is done using an analytical parameterization developed for in situ formed cirrus clouds and freezing fractions below 0.6 (Barahona and Nenes, 2009b). When the calculated freezing fraction exceeds 0.6, a sigmoidal increase in N_c is assumed (Barahona et al., 2010a),

in agreement with parcel model simulations and field observations (Barahona and Nenes, 2008; DeMott et al., 2003). For combined homogeneous and heterogeneous nucleation, it was assumed that the IN freeze instantaneously at a supersaturation freezing threshold, $s_{\rm het}$, of 15%, typical of deposition mode IN (Abbatt et al., 2006), with a 0.1 µm diameter at freezing (Froyd et al., 2009). Glassy aerosol was assumed to have a total concentration of 50 cm^{-3} and a freezing fraction given by the nucleation spectrum of Murray et al. (2010).

3.3.2 Vertical velocity spectrum

Observations suggest that the spectrum of gravity wave perturbations near the tropopause is pseudorandom in nature, a result of the superposition of waves from different sources, and therefore varies temporally and spatially (Bacmeister et al., 1999; Jensen and Pfister, 2004; Kim et al., 2003; Sato, 1990). On average, the associated vertical velocity spectrum can be approximated by a Gaussian function, although this may underestimate the frequency of high amplitude perturbations (Bacmeister et al., 1999; Herzog and Vial, 2001; Kim et al., 2003). A representative spectrum of vertical velocity fluctuations can be generated using a Fourier series (Bacmeister et al., 1999; Jensen and Pfister, 2004) of the form $u = \bar{u} + \sum_j A(\varpi_j)\cos(\varpi_j t + mH + \varphi)$ where m is the vertical wave number, H is the cloud thickness, and ϖ_j, $A(\varpi_j)$, and φ, are the wave frequency, phase, and amplitude, respectively. We have adopted this representation as follows. For each cirrus simulation, a time series of u was generated over the frequency interval $\varpi = [3.35\times10^{-7}, 9.44\times10^{-4}]$ Hz (Jensen and Pfister, 2004), using randomly generated φ and m. $A(\varpi_j)$ was calculated using a power spectrum scaling law of -1.85 for $\varpi_j > 1\times10^{-5}$ Hz and of -0.25 for $\varpi_j \le 1\times10^{-5}$ Hz (Herzog and Vial, 2001; Jensen and Pfister, 2004). This procedure resulted in a normal distribution of u (Fig. 4d) centered around $\bar{u}$. The maximum amplitude was assumed to occur at $\varpi_j = 1\times10^{-3}$ Hz (Jensen and Pfister, 2004) as it reproduces the results of Gayet et al. (2004) (Fig. 4 green line) which give positive u around 0.23 m s^{-1} for $\delta T = 1$ K (i.e., $A(1\times10^{-3}) \approx 2.1\delta T$). Representative time series for $u(t)$ are presented in Fig. 5a.

3.3.3 Ice crystal production

The homogeneous freezing timescale, $\tau_{{\rm hom},j}$, was calculated using the parameterization of Barahona and Nenes (2008, 2009b, a). Precursor aerosol was assumed to be composed of deliquesced ammonium sulfate, lognormally distributed with dry mean geometric diameter of 40 nm, geometric dispersion of 2.3, and number concentration of 100 cm^{-3} (Lawson et al., 2008). To account for possible compositional impacts on crystal growth kinetics, the water-vapor deposition coefficient was varied between 0.006 (Magee et al., 2006) and 1.0. Homogeneous freezing is described using the parameterization of Koop et al. (2000). The term $P_{\rm s}(S > S_{\rm hom})$ in Eq. (28) is the probability of finding S above $S_{\rm hom}$, and is introduced to account for the threshold behavior of homogeneous freezing (Kärcher and Burkhardt, 2008; Koop et al., 2000). The effect of preexisting ice crystals on freezing was accounted for by allowing a fraction of $N_{\rm c}$ to deplete water vapor and increase $\tau_{{\rm hom},j}$ (Barahona and Nenes, 2009b; Barahona et al., 2010b). The fraction of preexisting crystals remaining in freezing zones was calculated as $f_{\rm ps} = \frac{1}{N_{\rm c}\bar{D}_{\rm c}} \int_{D_{\rm min}}^{D_{\rm term}} D_{\rm c} n_{\rm c}(D_{\rm c}) dD_{\rm c}$, where $n(D_{\rm c})$ is the ice crystal size distribution, $D_{\rm min}$ is the minimum pre-existing crystal size, and $D_{\rm term}$ is the crystal size for which its terminal velocity, $u_{\rm term}$, is equal to the uplift velocity of the cirrus later, $\bar{u}$. $u_{\rm term}$ was calculated assuming ice crystals have columnar shape with maximum dimension equal to $\bar{D}_{\rm c}$ (Heymsfield and Iaquinta, 2000). Following Heymsfield and Platt (1984) it was assumed $n(D_{\rm c}) = AD_{\rm c}^{-3.15}$; the parameters A and $D_{\rm min}$ were calculated from the moments of $n(D_{\rm c})$: $N_{\rm c} = \int_{D_{\rm min}}^{\infty} n(D_{\rm c}) dD_{\rm c}$ and $\bar{D}_{\rm c} = \frac{1}{N_{\rm c}} \int_{D_{\rm min}}^{\infty} D_{\rm c} n(D_{\rm c}) dD_{\rm c}$. The calculation of $\bar{D}_{\rm c}$ is described below. Integration of equations of Eqs. (18) and (21) was accomplished using a fixed time step of 2 s. Initial values for $N_{{\rm c},0} = 0.01$ cm^{-3} and $S_{\rm o} = 1.0$ were set. Sensitivity to using different initial values affected only the time required to establish dynamic equilibrium (by a few hours) and is assessed in Fig. 8.

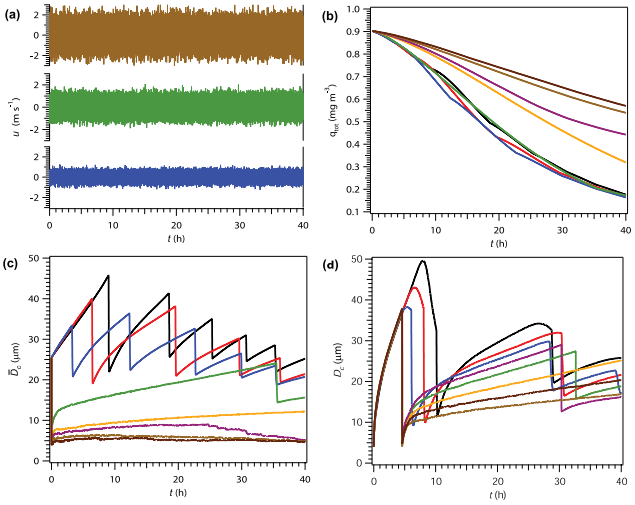

Fig. 5. Time series of **(a)** updraft velocity, u, **(b)** total water content, $q_{\rm tot}$, and $\bar{D}_{\rm c}$ **(c)** mean ice crystal diameter, $\bar{D}_{\rm c}$, for the conditions presented in Fig. 4; **(d)** time series of $\bar{D}_{\rm c}$ for initial S and $N_{\rm c}$ of -0.2 and 0, respectively, and homogeneous and heterogeneous nucleation active (conditions similar to Fig. 8c).

The heterogeneous freezing timescale, $\tau_{{\rm het},j}$, (e.g., Eq. 32) was calculated at each time step using the instantaneous vertical velocity, u_j, and the effective supersaturation $\overline{S}_{{\rm eff},j}$. For the simulations presented in Sect. 4, the aerosol freezing fraction, $f_{\rm het}$, was calculated from the spectrum of Murray et al. (2010). $N_{\rm o,het}$ and $S_{\rm het}$ were set to 1 cm^{-3} and 1.35, respectively (Murray et al., 2010).

3.3.4 Ice crystal sedimentation

The rate of ice crystal sedimentation over the cloud scale, H, was assumed proportional to the terminal velocity of the mean crystal size $\bar{D}_c$ (Eq. 33). Other removal processes (ice crystal sublimation and detrainment) are neglected; H however was varied over a wide interval (100 to 5000 m) to account for the uncertainty associated with neglecting these processes. $\bar{D}_c$ was calculated so that the total water vapor in the layer was partitioned between ice and vapor phases, i.e., $\bar{D}_c = \left(\frac{6q_{ice}}{\pi\rho_i N_c}\right)^{1/3}$ where $q_{ice} = q_{tot} - \frac{p^o S_o M_w}{RT}$, ρ_i is the ice density (Pruppacher and Klett, 1997), R is the universal gas constant, M_w is the molecular mass of water, and p^o is the saturation water vapor pressure over ice (Murphy and Koop, 2005); the minimum ice crystal size was set to 4 µm in agreement with theoretical studies and experimental observations (Barahona and Nenes, 2008; Durran et al., 2009; Krämer et al., 2009). Loss of total water content, q_{tot}, from the cloudy layer is also accounted for by solution of $\frac{dq_{tot}}{dt} = -\frac{\pi}{6}\rho_i \bar{D}_c^3 \frac{dN_c}{dt}\Big|_{sed}$. Representative time profiles of $\bar{D}_c$ and q_{tot} are presented in Fig. 5. The timescale of relaxation at $u = u_j$, $\tau_{rel,j}$, was calculated using N_c and $\bar{D}_c$ of the cloud layer (e.g., Eq. 13). Mass transfer limitation from non-continuum effects are taken into account in the calculation of $\tau_{hom,j}$ but neglected in the calculation of $\tau_{rel,j}$. The latter is justified as $\bar{D}_c > 10$ µm.

4 Cirrus in dynamical equilibrium

The model developed in Sect. 3 is used to describe the evolution of a cirrus layer at low temperature taking into account the effect of internal S variations on N_c. Forward integration of Eqs. (18) and (29) and (34) is carried out using the procedure described in Sect. 3.3. A wide range of initial conditions and model parameters are selected to describe the cirrus evolution under different scenarios.

Figure 4 shows the evolution of a cirrus layer subject to gravity-wave fluctuations with an initial average temperature of 195 K and lifting at $\bar{u} = 1\,\mathrm{cm\,s^{-1}}$. Only homogeneous freezing is considered (heterogeneous freezing is "switched off", i.e., $N_{o,het} = 0$). For values of $\delta T > 1$ K, the cloud initially experiences a strong homogeneous nucleation pulse, so that N_c initially increases steeply (Fig. 4a); the consumption of water vapor by crystal growth decreases S_o (Fig. 4b) which prevents any new freezing events. N_c slowly decreases from sedimentation loss; only after enough ice crystals sediment out of the cloud layer, S_o increases (e.g., $\delta T = 1$ K, green lines) and new freezing events occur. For $\delta T > 1.4$ K (purple lines) this is possible even if the layer remains on average slightly subsaturated ($S_o \sim 1$) because the probability distribution of S is broad enough for a non-negligible probability with $S > S_{hom}$. However it is likely that recently formed crystals will sublimate within a few hours in the subsaturated environment returning the moisture to the layer (ice crystal removal by sublimation is not considered). The cirrus is then maintained by new, independent freezing events. This "pulse-decay" behavior is characterized by $\tau_{sed} \gg \tau_{rel}$ so ice crystals reside long enough in the cloud to relax supersaturation (Fig. 4c); this behavior is also consistent with the parcel model concept of cirrus (where high N_c and low S_o coexist within the parcel). The subsaturation levels (Fig. 4b) achieved in this state are in agreement with in situ observations of relative humidity in dissipating clouds (Gao et al., 2004; Krämer et al., 2009).

The cirrus evolution is however quite different when δT is small; the distribution of S is narrow, and substantial ice production is only possible after enough supersaturation (i.e., S_o) builds up in the cloudy layer to allow a non-negligible probability where $S > S_{hom}$. Thus, freezing events producing large N_c (associated with large u fluctuations; Fig. 4d) are less frequent. Low N_c allows the formation of large ice crystals (Fig. 5c, d) which sediment out of the layer before substantially depleting supersaturation, leading to new freezing events. This "dynamic equilibrium" between ice production and loss is a previously unidentified microphysical regime of cirrus, characterized by $\tau_{sed} \sim \tau_{rel,j}$ (Fig. 4c); it maintains low N_c and high S_o in the cloudy layer (Fig. 4a, b) and is consistent with observations of low-temperature cirrus. Clouds in "dynamic equilibrium" also exhibit broad crystal size distribution, because large ice crystals coexist with freshly-formed (small) crystals in the cloud. The average ice crystal size in this case converges to values around 15 to 20 µm, in agreement with observations (Krämer et al., 2009). Before equilibrium is reached, D_c exhibits larger values due to the model's sensitivity to initial conditions (Fig. 5c, d).

When simulations (such as those of Fig. 4) are placed on a "state diagram" of N_c vs. S_o, the two microphysical regimes described above clearly emerge. Examples are presented in Figs. 6 and 7 for a range model parameters and a variety of δT (lines of distinct color). For example, decreasing the cloud thickness to 100 m (Fig. 4b) increases the sedimentation rate (Eq. 34) allowing S to replenish quickly and facilitating the onset of equilibrium. Similarly, the rate of ice crystal growth increases with T (Fig. 4d) increasing the average ice crystal size (hence decreasing τ_{rel} and τ_{sed}) and facilitating the onset of equilibrium. Dynamical equilibrium would however lead to lower N_c than observed at $T \sim 225$ K (Gayet et al., 2004; Krämer et al., 2009) and it is likely that clouds at these conditions would evolve following a pulse-decay behavior. Figure 7 shows state diagrams for different values of $\bar{u}$, T and H for the similar initial conditions. In general, progression towards a "dynamic equilibrium" is favored when supersaturation replenishes quickly (i.e., at high $\bar{u}$) as ice crystal growth and sedimentation are favored (leading to low τ_{sed}), and vice-versa for "pulse-decay" behavior. Rapid consumption of supersaturation by the growing ice crystals also decreases the time between freezing pulses and replenishment of S. Thus the period of the S and N_c oscillations in the dynamic equilibrium state is mainly controlled by τ_{rel}.

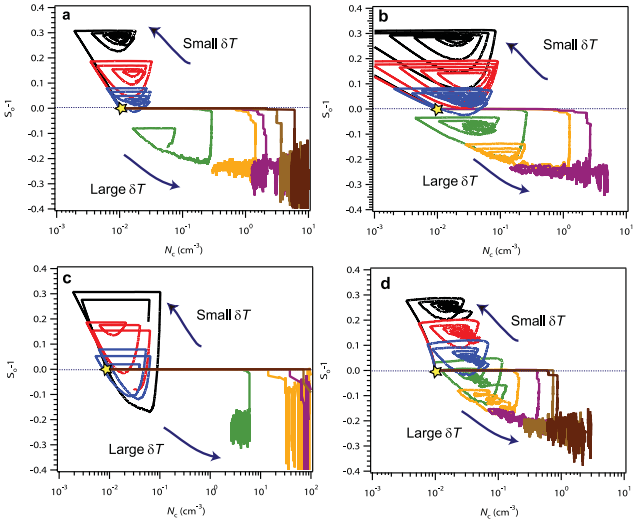

Fig. 6. Sensitivity of N_c and S_o evolution to cloud formation conditions for different values of δT (color scheme same as in Fig. 4); **(a)** same conditions as in Fig. 4, **(b)** cloud thickness, $H = 100$ m (increased ice crystal removal rate), **(c)** deposition coefficient equal to 0.006 (Magee et al., 2006) (slow water vapor transfer), and **(d)** initial temperature 225 K and cloud lifting at 5 cm s^{-1}. The yellow star in each panel indicates initial conditions. The arrows indicate the temporal progression along each trajectory. The integration time was 40 h cases, except in **(d)** were it was 15 h.

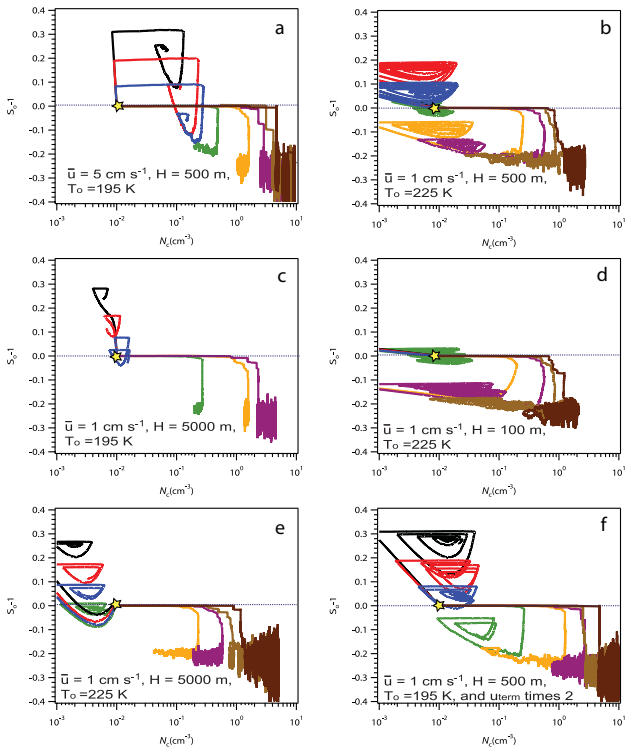

Fig. 7. Similar to Fig. 6, but varying cloud mean vertical velocity, $\bar{u}$, initial layer temperature, T_o, cloud thickness, H, and mean ice crystal terminal velocity, u_{term}. The yellow star in each plot indicates initial conditions. The integration time was 40 h in for $\bar{u} = 1$ cm s^{-1} and 15 h for $\bar{u} = 5$ cm s^{-1}.

Clouds in the "dynamic equilibrium" regime are also much less sensitive to slow water vapor deposition than predicted by box-model simulations. Figure 6c shows that dynamic equilibrium is possible even for α_d as low as 0.006 (compared to $\alpha_d = 1$ used in Figs. 4 and 6a for the same simulation conditions). Still, the high rate of production of ice crystals for $\alpha_d = 0.006$ increases N_c and decreases $\bar{D}_c$, therefore increasing τ_{sed} and slowing the replenishment of supersaturation. Thus, dynamic equilibrium is only possible for $\delta T < 0.8$ as opposed to $\delta T < 1.0$ for $\alpha_d = 1$. Figure 6c however shows that the existence of strong kinetic limitations to the diffusional growth of ice crystals cannot be ruled out.

4.1 Effect of heterogeneous IN and initial conditions

It is important to study the sensitivity of the dynamical states of cirrus to initial conditions used in the simulation and to the presence of heterogeneous IN. Figure 8a shows S and N_c for the conditions of Figs. 4 and 6a but starting at $S_{o,ini} = -0.4$ and $N_{c,o} = 0$. For this set of initial conditions, the onset of oscillating behavior is delayed by a few hours before supersaturation is reached. This implies that the temperature of the first freezing pulse is lower than in the case with $S_{o,ini} = 1$, slightly increasing its strength; the system however dampens out these variations and eventually follows a similar trajectory as in Fig. 6a.

Figure 8b and c present simulations where both homogeneous and heterogeneous nucleation are active for different initial conditions. IN are assumed to originate from glassy aerosol with $N_{o,het} = 1$ cm^{-3}. By allowing ice crystal formation at low S, heterogeneous IN decrease the ice crystal production rate by homogeneous nucleation hence lower the maximum N_c. This makes the system more stable to high amplitude vertical velocity perturbations, facilitating the onset of dynamic equilibrium, which can be maintained up to $\delta T \sim 1.2$. The "stabilizing" effect of IN is exemplified in Fig. 8c where homogeneous freezing was suppressed, i.e., only heterogeneous freezing is active. This leads to a dampened response to vertical velocity fluctuations so that dynamical equilibrium is possible even for δT as high as 1.8 K. Thus, in a cirrus cloud where heterogeneous nucleation is dominant, dynamical equilibrium is very robust against external perturbations. The values of N_c and S at the equilibrium state are however not significantly influenced by the initial conditions nor the ice nucleation mechanism, e.g., after sometime the system oscillates about the same values as in Figs. 6 and 7. This means that the presence of IN can "help" the cirrus to achieve dynamical equilibrium without modifying the equilibrium values.

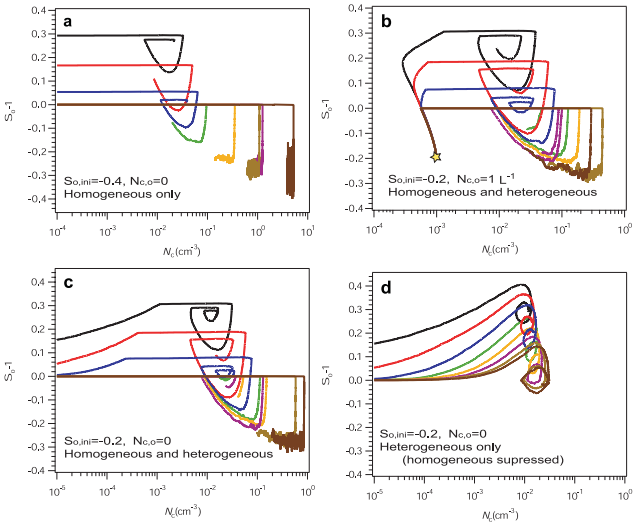

Fig. 8. Similar to Fig. 6, varying initial S and N_c and the active freezing mechanism.

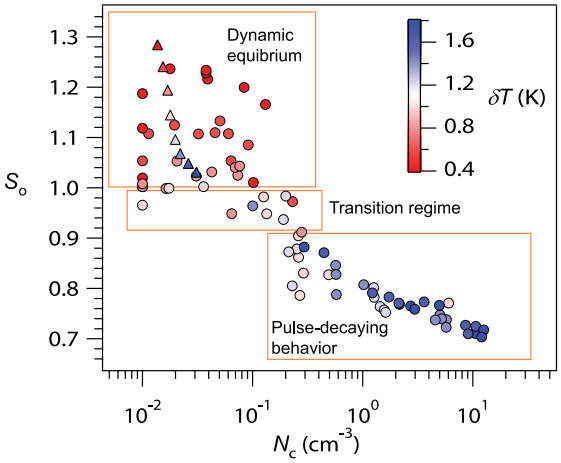

Fig. 9. Maximum ice crystal concentration obtained during the cloud evolution simulations against the time-averaged mean saturation ratio. Results presented for all simulations carried out in this study. Integration time varied between 15 and 40 h. Symbols are colored by the value of δT used. Regions where the cloud spontaneously transitions to a "pulse-decay" and "dynamic equilibrium" state are noted; the "transitional" region marks where the cloud generally initially exhibited "pulse-decay" behavior over few hours and then transitioned to a "dynamic equilibrium" regime. (◯) Homogeneous freezing is active; (△) Homogeneous freezing suppressed.

Figures 6 to 8 also show that the "dynamic equilibrium" state occurs spontaneously when δT goes below a characteristic transition value (which depends on $\bar{u}$, T and the predominant freezing mechanism). It can also be reached after a cloud initially resides in a "pulse-decay" state, if δT is close to the characteristic value ($\delta T \sim 1$ K in Fig. 6). When maximum N_c and time-averaged S_o are presented on the state diagram for all simulations considered where homogeneous freezing is active, the conditions of δT that separate "pulse-decay" and "dynamic equilibrium" regimes seem to be universal (Fig. 9). If only heterogeneous nucleation is active, the cloud resides mostly in the dynamic equilibrium state.

5 Conclusions and implications

From the discussion above, cold cirrus clouds will reside in the "dynamic equilibrium" regime if δT is below a characteristic threshold. High-amplitude, orographically-generated gravity waves are ubiquitous (Kim et al., 2003) but often lose intensity with altitude, weakening their contribution to the background spectrum of temperature fluctuations. δT can thus decrease enough at high altitude for cirrus to transition from a "pulse-decay" to a "dynamic equilibrium" state (Fig. 9). This would explain why low N_c and high S_o are observed at low temperatures near the tropopause. Dynamical equilibrium is also possible at warmer conditions (particularly for high $\bar{u}$; Fig. 6d) but require small δT; given that high amplitude fluctuations are widespread at lower altitudes (Hoyle et al., 2005), cirrus clouds are likely forced to always follow a pulse-decaying behavior. Heterogeneous IN nevertheless may help to stabilize the system so that the dynamic equilibrium manifests at higher δT than for clouds with pure homogeneous freezing.

In summary, cirrus clouds at low temperature exhibit characteristics (e.g., low N_c and sustained high saturation ratios) that cannot be explained with the simple "conventional" picture of homogeneous freezing driven by expansion cooling in the presence of ubiquitous temperature fluctuations. Even if heterogeneous nucleation is dominant, conventional models of cirrus could explain the characteristics of low-T cirrus only for weak updrafts, and require neglecting the higher amplitude components of the vertical velocity spectrum. Instead, we show that small-scale fluctuations from the action of gravity waves can switch a cloud into a previously unknown "dynamic equilibrium" regime, with sustained levels of low N_c and high saturation ratios consistent with "puzzling" characteristics observed in low temperature cirrus.

With this study, a new understanding for cirrus clouds emerges, where the "unperturbed" microphysical state is one of dynamical equilibrium with low crystal number and high supersaturation. Only when the mean amplitude of temperature fluctuations exceeds a threshold value ($\delta T \sim 1$ K when homogeneous freezing is active) cirrus exhibit the well-known "pulse-decay" microphysical state. Throughout much of the atmosphere, the latter state dominates, simply because δT is larger than the characteristic threshold value. In the TTL, δT is still remarkably large (0.6–0.8 K) (Bacmeister et al., 1999; Jensen and Pfister, 2004; Sato, 1990), but does not systematically exceed the threshold for "pulse-decay" behavior, so cirrus regress to their "unperturbed" dynamic-equilibrium state. The presence of heterogeneous IN can

also dampen the effect of vertical velocity perturbations on ice crystal production facilitating the transition to dynamic equilibrium. However, the existence of IN is not a necessary condition to explain the characteristics of cirrus clouds at low temperature. Figure 6c shows that dynamic equilibrium states can also exist even under conditions of strong kinetic limitations (very low α_d) and therefore their existence cannot be ruled out based on simplified models of cirrus formation.

The structure and responses of cirrus to dynamical and microphysical forcings can also be portrayed. For example, cirrus formed in the region of convective anvils might exhibit "pulse-decay" state until gravity-wave fluctuations decay to below the δT threshold and transition to a dynamic-equilibrium state. For the same reasons, IN impacts on cirrus properties can be strong for clouds in pulse-decay state, but not for clouds in dynamic equilibrium; e.g., IN can force the cloud to fall towards equilibrium however will not modify the equilibrium state. In conclusion, the discovery of dynamic equilibrium states reshapes our understanding of cirrus clouds and their role in anthropogenic climate change, as the type of dynamical forcing and the presence of IN will set these clouds in one of two "preferred" microphysical regimes with very different susceptibility to anthropogenic aerosol.

Acknowledgements. This study was supported by NASA ACMAP and a NSF CAREER award.

Edited by: J. H. Seinfeld

References

Abbatt, J. P. D., Benz, S., Cziczo, D. J., Kanji, Z., and Möhler, O.: Solid ammonium sulfate as ice nuclei: a pathway for cirrus cloud formation, Science, 313, 1770–1773, 2006.

Bacmeister, J., Eckermann, S. D., Tsias, A., Carslaw, K. S., and Peter, T.: Mesoscale temperature fluctuations induced by a spectrum of gravity waves: A comparison of parameterizations and their impact on stratospheric microphysics, J. Atmos. Sci., 56, 1913–1924, 1999.

Barahona, D. and Nenes, A.: Parameterization of cloud droplet formation in large scale models: including effects of entrainment, J. Geophys. Res., 112, D16026; doi:16010.11029/16207JD008473, 2007.

Barahona, D. and Nenes, A.: Parameterization of cirrus formation in large scale models: Homogeneous nucleation, J. Geophys. Res., 113, D11211, doi:11210.11029/12007JD009355, 2008.

Barahona, D. and Nenes, A.: Parameterizing the competition between homogeneous and heterogeneous freezing in ice cloud formation polydisperse ice nuclei, Atmos. Chem. Phys., 9, 5933–5948, doi:10.5194/acp-9-5933-2009, 2009a.

Barahona, D. and Nenes, A.: Parameterizing the competition between homogeneous and heterogeneous freezing in cirrus cloud formation - monodisperse ice nuclei, Atmos. Chem. Phys., 9, 369–381, doi:10.5194/acp-9-369-2009, 2009b.

Barahona, D., Rodriguez, J. M., and Nenes, A.: Sensitivity of the global distribution of cirrus Ice crystal concentration to heterogeneous freezing, J. Geophys. Res., 115, D23213, doi:23210.21029/22010JD014273, 2010a.

Barahona, D., West, R. E. L., Stier, P., Romakkaniemi, S., Kokkola, H., and Nenes, A.: Comprehensively accounting for the effect of giant CCN in cloud activation parameterizations, Atmos. Chem. Phys., 10, 2467–2473, doi:10.5194/acp-10-2467-2010, 2010b.

DeMott, P. J., Meyers, M. P., and Cotton, R. W.: Parameterization and impact of ice initiation processes relevant to numerical model simulations of cirrus clouds, J. Atmos. Sci., 51, 77–90, 1994.

DeMott, P. J., Cziczo, D. J., Prenni, A. J., Murphy, D. M., Kreidenweis, S. M., Thompson, D. S., Borys, R., and Rogers, D. C.: Measurements of the concentration and composition of nuclei for cirrus formation, Proc. Natl. Acad. Sci. USA, 100, 14655–14660, 2003.

Durran, D. R., Dinh, T., Ammerman, M., and Ackerman, T.: The mesoscale dynamics of thin tropical tropopause cirrus, J. Atmos. Sci., 66, 2859–2873, doi:10.1175/2009JAS3046.1, 2009.

Fountoukis, C. and Nenes, A.: ISORROPIA II: a computationally efficient thermodynamic equilibrium model for $K^+Ca^{2+}Mg2+NH_4^+Na^+SO_4^{2-}NO_3^-Cl^-H_2O$ aerosols, Atmos. Chem. Phys., 7, 4639–4659, doi:10.5194/acp-7-4639-2007, 2007.

Froyd, K. D., Murphy, D. M., Sanford, T. J., Thomson, D. S., Wilson, J. C., Pfister, L., and Lait, L.: Aerosol composition of the tropical upper troposphere, Atmos. Chem. Phys., 9, 4363–4385, doi:10.5194/acp-9-4363-2009, 2009.

Gao, R. S., Popp, P. J., Fahey, D. W., Marcy, T. P., Herman, R. L., Weinstock, E. M., Baumgardner, D. G., Garrett, T. J., Rosenlof, K. H., Thompson, T. L., Bui, P. T., Ridley, B. A., Wofsy, S. C., Toon, O. B., Tolbert, M. A., Kärcher, B., Peter, T., Hudson, P. K., Weinheimer, A. J., and Heymsfield, A. J.: Evidence that nitric acid increases relative humidity in low-temperature cirrus clouds, Science, 303, 516–520, 2004.

Gayet, J. F., Ovarlez, J., Shcherbakov, V., Ström, J., Schumann, U., Minikin, A., Auriol, F., Petzold, A., and Monier, M.: Cirrus cloud microphysical and optical properties at southern and northern midlatitudes during the INCA experiment, J. Geophys. Res., 109, D20206, doi:20210.21029/22004JD004803, 2004.

Gensch, I. V., Bunz, H., Baumgardner, D. G., Christensen, L. E., Fahey, D. W., Herman, R. L., Popp, P. J., Smith, J. B., Troy, R. F., Webster, C. R., Weinstock, E. M., Wilson, J., Peter, T., and Krämer, M.: Supersaturations, microphysics and nitric acid partitioning in a cold cirrus cloud observed during CR-AVE 2006: an observation-modelling intercomparison study, Environ. Res. Lett., 3, 035003, doi:10.1088/1748-9326/3/3/035003, 2008.

Haag, W., Kärcher, B., Ström, J., Minikin, A., Lohmann, U., Ovarlez, J., and Stohl, A.: Freezing thresholds and cirrus cloud formation mechanisms inferred from in situ measurements of relative humidity, Atmos. Chem. Phys., 3, 1791–1806, doi:10.5194/acp-3-1791-2003, 2003.

Herzog, A. and Vial, F.: A study of the dynamics of the equatorial lower stratosphere by use of ultra-long-duration balloons, J. Geophys. Res., 106, 22745–22761, 2001.

Heymsfield, A. J. and Platt, C. M.: A parameterization of the particle size spectrum of ice clouds in terms of the ambient temperature and ice water content, J. Atmos. Sci., 41, 846–855, 1984.

Heymsfield, A. J. and Sabin, R. M.: Cirrus crystal nucleation by homogenous freezing of solution droplets., J. Atmos. Sci., 46,

2252–2264, 1989.

Heymsfield, A. J. and Iaquinta, J.: Cirrus crystals terminal velocities, J. Atmos. Sci., 57, 916–938, 2000.

Hoyle, C. R., Luo, B. P., and Peter, T.: The origin of high ice crystal number densities in cirrus clouds, J. Atmos. Sci., 62, 2658–2579, 2005.

Jensen, E. J. and Pfister, L.: Transport and freeze-drying in the tropical tropopause layer, J. Geophys. Res., 109, D02207, doi:02210.01029/02003JD004022, 2004.

Jensen, E. J., Smith, J. B., Pfister, L., Pittman, J. V., Weinstock, E. M., Sayres, D. S., Herman, R. L., Troy, R. F., Rosenlof, K., Thompson, T. L., Fridlind, A. M., Hudson, P. K., Cziczo, D. J., Heymsfield, A. J., Schmitt, C., and Wilson, J. C.: Ice supersaturations exceeding 100% at the cold tropical tropopause: implications for cirrus formation and dehydration, Atmos. Chem. Phys., 5, 851–862, doi:10.5194/acp-5-851-2005, 2005.

Jensen, E. J., Pfister, L., Bui, T. V., Lawson, P., Baker, B., Mo, Q., Baumgardner, D., Weinstock, E. M., Smith, J. B., Moyer, E. J., Hanisco, T. F., Sayres, D. S., Clair, J. M. St., Alexander, M. J., Toon, O. B., and Smith, J. A.: Formation of large ($\simeq$100 µm) ice crystals near the tropical tropopause, Atmos. Chem. Phys., 8, 1621–1633, doi:10.5194/acp-8-1621-2008, 2008.

Jensen, E. J., Pfister, L., Bui, T.-P., Lawson, P., and Baumgardner, D.: Ice nucleation and cloud microphysical properties in tropical tropopause layer cirrus, Atmos. Chem. Phys., 10, 1369–1384, doi:10.5194/acp-10-1369-2010, 2010.

Kärcher, B. and Burkhardt, U.: A cirrus scheme for global circulation models, Q. J. Roy. Meteorol. Soc., 134, 1439–1461; doi:1410.1002/Qj.1301, 2008.

Kärcher, B. and Lohmann, U.: A parameterization of cirrus cloud formation: homogeneous freezing of supercooled aerosols, J. Geophys. Res., 107, 4010, doi:4010.1029/2001JD000470, 2002.

Kärcher, B. and Haag, W.: Factors controlling upper tropospheric relative humidity, Ann. Geophys., 22, 705–715, doi:10.5194/angeo-22-705-2004, 2004.

Kärcher, B., Hendricks, J., and Lohmann, U.: Physically based parameterization of cirrus cloud formation for use in global atmospheric models, J. Geophys. Res., 111, D01205, doi:01210.01029/02005JD006219, 2006.

Kay, J. E., Baker, M., and Hegg, D.: Physical controls on orographic cirrus inhomogeneity, Atmos. Chem. Phys., 7, 3771–3781, doi:10.5194/acp-7-3771-2007, 2007.

Khvorostyanov, V. I., Morrison, H., Curry, J. A., Baumgardner, D. G., and Lawson, P.: High supersaturation and modes of ice nucleation in thin tropopause cirrus: simulation of the 13 July 2002 cirrus regional study of tropical anvils and cirrus layers case, J. Geophys. Res., 111, D02201, doi:02210.01029/02004JD005235, 2006.

Kim, Y.-J., Eckermann, S. D., and Chun, H.-Y.: An overview of the past, present, and future of gravity-wave drag parameterization for numerical climate and weather prediction models, Atmos.-Ocean, 41, 65–98, 2003.

Koop, T., Luo, B., Tslas, A., and Peter, T.: Water activity as the determinant for homogeneous ice nucleation in aqueous solutions, Nature, 406, 611–614, 2000.

Korolev, A. V. and Mazin, I. P.: Supersaturation of water vapor in clouds, J. Atmos. Sci., 60, 2957–2974, 2003.

Krämer, M., Schiller, C., Afchine, A., Bauer, R., Gensch, I., Mangold, A., Schlicht, S., Spelten, N., Sitnikov, N., Borrmann, S., de Reus, M., and Spichtinger, P.: Ice supersaturations and cirrus cloud crystal numbers, Atmos. Chem. Phys., 9, 3505–3522, doi:10.5194/acp-9-3505-2009, 2009.

Lawson, R. P., Pilson, B., Baker, B., Mo, Q., Jensen, E., Pfister, L., and Bui, P.: Aircraft measurements of microphysical properties of subvisible cirrus in the tropical tropopause layer, Atmos. Chem. Phys., 8, 1609–1620, doi:10.5194/acp-8-1609-2008, 2008.

Liou, K.: Influence of cirrus clouds on weather and climate processes: a global perspective, Mon. Weather Rev., 114, 1167–1199, 1986.

Lohmann, U. and Feichter, J.: Global indirect aerosol effects: a review, Atmos. Chem. Phys., 5, 715–737, doi:10.5194/acp-5-715-2005, 2005.

Magee, N., Moyle, A. M., and Lamb, D.: Experimental determination of the deposition coefficient of small cirrus-like ice crystals near $-50\,^{\circ}$C, Geophys. Res. Lett., 33, L17813, doi:17810.11029/12006GL026665, 2006.

Murray, B. J.: Inhibition of ice crystallisation in highly viscous aqueous organic acid droplets, Atmos. Chem. Phys., 8, 5423–5433, doi:10.5194/acp-8-5423-2008, 2008.

Murphy, D. M. and Koop, T.: Review of the vapour pressures of ice and supercooled water for atmospheric applications, Q. J. Roy. Meteorol. Soc., 131, 1539–1565, 2005.

Murray, B. J., Knopf, D. A., and Bertram, A. K.: The formation of cubic ice under conditions relevant to Earth's atmosphere, Nature, 434, 202–205, 2005.

Murray, B. J., Wilson, T. W., Dobbie, S., Cui, Z., Al-Jumur, S. M. R. K., Möhler, O., Schnaiter, M., Wagner, R., Benz, S., Niemand, M., Saathoff, H., Ebert, V., Wagner, S., and Kärcher, B.: Heterogeneous nucleation of ice particles on glassy aerosol under cirrus conditions, Nature Geosci., 3, 233–237, 2010.

Peter, T.: Microphysics and heterogeneous chemistry of polar stratospheric clouds Annu. Rev. Phys. Chem., 48, 785–822, 1997.

Peter, T., Marcolli, C., Spichtinger, P., Corti, T., Baker, B., and Koop, T.: When dry air is too humid, Science, 314, 1399–1401, 2006.

Pruppacher, H. R. and Klett, J. D.: Microphysics of clouds and precipitation 2nd ed., Kluwer Academic Publishers, Boston, MA, 954 pp., 1997.

Ramanathan, V. and Collins, W.: Thermodynamic regulation of ocean warming by cirrus clouds deduced from observations of 1987 El Nino, Nature, 351, 27–32, 1991.

Sato, K.: Vertical wind disturbances in the troposphere and lower stratosphere observed by the MU radar, J. Atmos. Sci., 47, 2803–2817, 1990.

Seinfeld, J. H.: Clouds, contrails and climate, Nature, 391, 837–838, 1998.

Seinfeld, J. H. and Pandis, S. N.: Atmospheric Chemistry and Physics, John Wiley and Sons, New York, NY, USA, 1998.

Selkirk, H. B., Vömel, H., Valverde Canossa, J. M., Pfister, L., Diaz, J. A., Fernández, W., Amador, J., Stolz, W., and Peng, G. S.: Detailed structure of the tropical upper troposphere and lower stratosphere as revealed by balloon sonde observations of water vapor, ozone, temperature, and winds during the NASA TCSP and TC4 campaigns, J. Geophys. Res., 115, D00J19, doi:10.1029/2009jd013209, 2010.

Shilling, J. E., Fortin, T. J., and Tolbert, M. A.: Depositional ice nu-

cleation on crystalline organic and inorganic solids, J. Geophys. Res., 111, D12204; doi:12101.11029/12005JD006664, 2006.

Spichtinger, P. and Gierens, K. M.: Modelling of cirrus clouds – Part 2: Competition of different nucleation mechanisms, Atmos. Chem. Phys., 9, 2319–2334, doi:10.5194/acp-9-2319-2009, 2009a.

Spichtinger, P. and Gierens, K. M.: Modelling of cirrus clouds – Part 1b: Structuring cirrus clouds by dynamics, Atmos. Chem. Phys., 9, 707–719, doi:10.5194/acp-9-707-2009, 2009b.

Wise, M. E., Baustian, K. J., and Tolbert, M. A.: Internally mixed sulfate and organic particles as potential ice nuclei in the tropical tropopause region, 107, 6693–6698, doi:6610.1073/pnas.0913018107, 2010.